JOURNAL OF SPACECRAFT AND ROCKETS
Vol. 45, No. 2, March–April 2008

Orbital Dynamics of Solar Sails for Geomagnetic Tail Exploration

Teppei Oyama,* Hiroshi Yamakawa,† and Yoshiharu Omura‡
Kyoto University, Uji, Kyoto 611-0011, Japan

DOI: 10.2514/1.31274

The orbital dynamics of Earth-orbiting solar sails is investigated considering an artificial apse-line precession of an elliptic orbit by solar radiation pressure. The orbital coverage can be flexibly designed for missions such as geomagnetic tail exploration by allowing eccentricity variation via an extremely simple steering law in which the sail normal is set to be directed along the sun line at all times. Equations describing the long-term behavior of eccentricity and argument of perigee are derived by averaging Lagrange's planetary equations constituting a Hamiltonian system. The canonical transformation approach is also shown to yield the same equations. The Hamiltonian of the system makes it possible to investigate the temporal evolution of the eccentricity and the argument of perigee in terms of an eccentricity argument of a perigee phase-space diagram. Orbits in phase space are shown to be classifiable as librational, rotational, or unstable, depending on the magnitude of the characteristic acceleration of the solar sail. The librational dynamics of a solar sail are applied numerically to the case of geomagnetic tail observations.

Nomenclature

a	=	normalized semimajor axis
a_0	=	normalized characteristic acceleration of the solar sail
e	=	eccentricity
e_1, e_2	=	extreme eccentricities
$F(H, \bar{k})$	=	area of closed orbits in $(\bar{k}, \bar{\gamma})$ phase space
f_r, f_θ	=	normalized radial and transverse components of solar radiation on the solar sail
f_x, f_y	=	normalized x and y components of solar radiation on the solar sail in the inertial frame
H	=	Hamiltonian
H'	=	H/β
H_0	=	Hamiltonian for the unperturbed Hamiltonian system
$\mathbf{J}$	=	vector form of action variables
J_i	=	action variables (Delaunay variables with $i = 1, 2$)
K	=	Hamiltonian after canonical transformation
$\bar{k}$	=	$\sqrt{1-(\bar{e})^2}$
$\bar{k}_0$	=	$\bar{k}$ of equilibrium point in $(\bar{k}, \bar{\gamma})$ phase space
$\bar{k}_\pm$	=	value of $\bar{k}$ at two intersections of the curve $F(H, \bar{k})$ with $\bar{\gamma} = 0$
M	=	mean anomaly
$\mathbf{p}, \mathbf{P}$	=	generalized momenta
$\mathbf{q}, \mathbf{Q}$	=	generalized coordinates
r	=	normalized distance
T	=	normalized period of closed orbits in $(\bar{k}, \bar{\gamma})$ phase space
t	=	normalized time
$\mathbf{w}$	=	vector form of angle variables
w_i	=	angle variables
α	=	solar pressure parameter
β_0	=	average normalized orbital rate of the Earth
$\bar{\gamma}$	=	$\bar{\omega} - \beta_0 t$
$\bar{\gamma}_0$	=	$\bar{\gamma}$ of equilibrium point in $(\bar{k}, \bar{\gamma})$ phase space
ΔH	=	perturbation Hamiltonian
θ	=	true anomaly
θ'	=	$\theta - \omega$
Σ	=	angular position of the sun from vernal equinox
ψ	=	eccentric anomaly
ω	=	argument of perigee
$\bar{}$	=	(overbar) averaged value over a single revolution

Received 27 March 2007; revision received 29 August 2007; accepted for publication 9 September 2007.

*Graduate Student, Graduate School of Engineering, Department of Electrical Engineering; currently at Fujitsu, Ltd.; oyama@rish.kyoto-u.ac.jp.

†Professor, Research Institute for Sustainable Humanosphere, Division of Creative Research and Development of Humanosphere; yamakawa@rish.kyoto-u.ac.jp. Senior Member AIAA.

‡Professor, Research Institute for Sustainable Humanosphere, Division of Creative Research and Development of Humanosphere; omura@rish.kyoto-u.ac.jp.

I. Introduction

SOLAR-SAIL technology has been widely investigated as a means of using solar radiation pressure as a propulsive force [1]. A solar sail is a large, thin film that provides thrust derived from solar radiation, thus eliminating the need for fuel. High-energy space science missions, such as interplanetary and solar probe missions, may be realized using solar-sail propulsion [2–5], and new observation points for solar physics and space science applications may become available [6–8].

McInnes et al. [9] and MacDonald and McInnes [10] have proposed the Geosail mission for observing the geomagnetic tail of the Earth by an artificial apse-line precession of an elliptical orbit under solar radiation pressure propulsion. The artificial precession of the apse line of an elliptic orbit with major axis oriented in the sun–Earth line thus achieves consecutive coverage of the geomagnetic tail. The geomagnetic tail is an elongated electromagnetic structure formed by interaction of the solar wind with the intrinsic magnetic field of the Earth. As the apse line of the Keplerian elliptic orbit is fixed inertially, useful scientific data can only be collected in the geomagnetic tail once each year. Far-field observations of the geomagnetic tail outside the lunar orbit have been successfully realized by the GEOTAIL spacecraft [11], which was launched in 1992 and uses multiple lunar swingbys. However, consecutive observations of near field inside the lunar orbit is hardly realized using a Keplerian elliptic orbit. The proposed Geosail mission [9,10] involves a 10×30 Earth radii elliptic orbit and the use of a small solar sail to artificially precess the apse line at a rate of 0.9856 deg/day in order to track the annual rotation of the geomagnetic tail. The sail steering law is such that sail normal is to be directed along the major axis of the ellipse, fixing the eccentricity of the Geosail orbit.

In the present study, the scientific return of a Geosail mission is extended by relaxing the fixed eccentricity condition to allow wider coverage of the geomagnetic tail by simply pointing the sail normal

toward the sun. The long-term evolution of the solar-sail orbit is obtained by averaging Lagrange's planetary equations constituting a Hamiltonian system, the Hamiltonian of which gives the temporal evolution of the orbit in the eccentricity argument of perigee phase space.

II. Hamiltonian Approach Using Averaged Lagrange's Planetary Equations

The orbital geometry considered here is shown in Fig. 1. The sail normal is always pointed toward the sun, and the solar-sail orbits within the ecliptic plane. The acceleration exerted on the solar sail due to solar radiation pressure therefore lies in the ecliptic plane as described by

$$f_r = -a_0 \cos(\omega + \theta - \Sigma) \tag{1}$$

$$f_\theta = a_0 \sin(\omega + \theta - \Sigma) \tag{2}$$

where f_r and f_θ are the radial and transverse components of the solar radiation pressure on the solar sail (directed positively in the sense of spacecraft motion, negative in Fig. 1), a_0 is the normalized characteristic acceleration of the solar sail, ω is the argument of perigee, θ is the true anomaly of the solar-sail position, and Σ is the position of the sun from the vernal equinox (x). The characteristic acceleration is defined as the acceleration experienced by the solar sail at a heliocentric distance of 1 astronomical unit (AU) with the sail normal directed along the sun line. The characteristic acceleration is normalized by the Earth's gravitational force at the radius of the reference orbit. The effect of lunar and solar gravitational perturbations and higher-order geopotential will be discussed later. Defining the averaged nondimensional orbital rate of the Earth as β_0 (dimensional value: 0.9856 deg /day) and the initial time as that corresponding to the time point at which the sun is in the direction of the vernal equinox, the direction of the sun is given by

$$\Sigma = \beta_0 t$$

The in-plane solar radiation pressure is investigated using the following three normalized Lagrange equations [12]:

$$\frac{\mathrm{d}a}{\mathrm{d}\theta} = \frac{2ar^2}{(1-e^2)}\{f_r e \sin\theta + f_\theta(1 + e\cos\theta)\} \tag{3}$$

$$\frac{\mathrm{d}e}{\mathrm{d}\theta} = r^2\left\{f_r \sin\theta + f_\theta\left(\cos\theta + \frac{e + \cos\theta}{1 + e\cos\theta}\right)\right\} \tag{4}$$

$$\frac{\mathrm{d}\omega}{\mathrm{d}\theta} = \frac{r^2}{e}\left\{-f_r \cos\theta + f_\theta\left(1 + \frac{1}{1 + e\cos\theta}\right)\sin\theta\right\} \tag{5}$$

where r, a, and e are the distance between the solar sail and the Earth, the length of the semimajor axis, and the eccentricity. All the variables in Eqs. (3–5) are normalized with respect to the radius of the reference circular orbit, the corresponding period, and the Earth's gravitational force at the radius of the reference orbit. The normalization typically sets the reference terms in the denominator to 1.

The orbit of the solar sail under the influence of solar radiation pressure can be obtained by substituting Eqs. (1) and (2) into Eqs. (3–5). The long-term behavior of the solar-sail orbit can be best characterized by averaging Lagrange's planetary equations over a single revolution, which can be obtained as follows:

$$\begin{aligned}\overline{\frac{\mathrm{d}a}{\mathrm{d}t}} &= \frac{1}{2\pi\sqrt{a^3}}\int_0^{2\pi}\frac{\mathrm{d}a}{\mathrm{d}\theta}\mathrm{d}\theta = 0\\ \overline{\frac{\mathrm{d}e}{\mathrm{d}t}} &= \frac{1}{2\pi\sqrt{a^3}}\int_0^{2\pi}\frac{\mathrm{d}e}{\mathrm{d}\theta}\mathrm{d}\theta = \frac{3}{2}a_0\sqrt{\bar{a}}\sin(\bar{\omega} - \Sigma)\sqrt{1-(\bar{e})^2}\end{aligned} \tag{6}$$

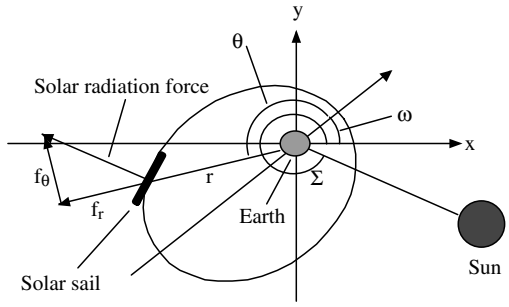

Fig. 1 Orbit geometry for solar sail.

$$\overline{\frac{\mathrm{d}\omega}{\mathrm{d}t}} = \frac{1}{2\pi\sqrt{a^3}}\int_0^{2\pi}\frac{\mathrm{d}\omega}{\mathrm{d}\theta}\mathrm{d}\theta = \frac{3}{2}a_0\sqrt{\bar{a}}\cos(\bar{\omega} - \Sigma)\frac{\sqrt{1-(\bar{e})^2}}{\bar{e}} \tag{7}$$

Here $\overline{\mathrm{d}a}/\mathrm{d}t$, $\overline{\mathrm{d}e}/\mathrm{d}t$, and $\overline{\mathrm{d}\omega}/\mathrm{d}t$ represent the averaged rates of change of the semimajor axis, eccentricity, and the argument of the perigee over a single revolution. In the integration, changes in orbit elements are neglected, and the average values of orbit elements ($\bar{a}$, $\bar{e}$, $\bar{\omega}$) are used on the right-hand side. Note that the repeated short-duration eclipses that have little effect on the required solar-sail performance are neglected as discussed in p. 624 of [9]. Applying the time-dependent transformation, $\bar{\gamma} = \bar{\omega} - \beta_0 t$, to Eqs. (6) and (7) yields

$$\begin{aligned}\overline{\frac{\mathrm{d}e}{\mathrm{d}t}} &= \frac{3}{2}a_0\sqrt{\bar{a}}\sin\bar{\gamma}\sqrt{1-(\bar{e})^2}\\ \overline{\frac{\mathrm{d}\gamma}{\mathrm{d}t}} &= \frac{3}{2}a_0\sqrt{\bar{a}}\cos\bar{\gamma}\frac{\sqrt{1-(\bar{e})^2}}{\bar{e}} - \beta_0\end{aligned}$$

These equations can be shown to constitute a Hamiltonian system by the transformation, $\bar{k} = \sqrt{1-(\bar{e})^2}$, where $\bar{k}$ represents a new variable corresponding to eccentricity. Applying this transformation affords the following autonomous Hamiltonian system:

$$\overline{\frac{\mathrm{d}\gamma}{\mathrm{d}t}} = \frac{3}{2}a_0\sqrt{\bar{a}}\cos\bar{\gamma}\frac{\bar{k}}{\sqrt{1-(\bar{k})^2}} - \beta_0 = \frac{\partial H}{\partial \bar{k}} \tag{8}$$

$$\overline{\frac{\mathrm{d}k}{\mathrm{d}t}} = -\frac{3}{2}a_0\sqrt{\bar{a}}\sin\bar{\gamma}\sqrt{1-(\bar{k})^2} = -\frac{\partial H}{\partial \bar{\gamma}} \tag{9}$$

where H represents the Hamiltonian of Eqs. (8) and (9), as given by

$$H = -\frac{3}{2}a_0\sqrt{\bar{a}}\sqrt{1-(\bar{k})^2}\cos\bar{\gamma} - \beta_0\bar{k} \tag{10}$$

As the Hamiltonian of the autonomous system is conservative, Eq. (10) gives the behavior of the satellite orbit in the $\bar{k} - \bar{\gamma}$ phase space. The same Hamiltonian can be derived by a canonical transformation approach, as detailed in the Appendix, where the manipulations required for averaging are substantially reduced.

III. Eccentricity Argument of Perigee Phase Space

The solar pressure parameter α is defined as follows:

$$\alpha = \frac{3a_0\sqrt{\bar{a}}}{2\beta_0} \tag{11}$$

Equation (10) can then be expressed in terms of α as follows:

$$\cos\bar{\gamma} = \frac{-H' - \bar{k}}{\alpha\sqrt{1-(\bar{k})^2}} \tag{12}$$

where $H' = H/\beta_0$. Equation (12) allows a solution curve to be constructed for various H' in $\bar{k} - \bar{\gamma}$ phase space, as shown in Fig. 2. In

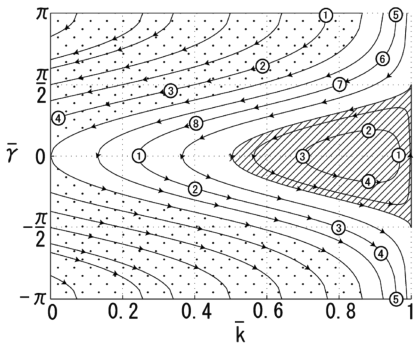

Fig. 2 Eccentricity argument of perigee phase-space diagram ($\alpha = 0.575$) showing librational (hatched, Fig. 3), rotational (unpatterned, Fig. 4), and unstable (dotted, Fig. 5) orbital regions.

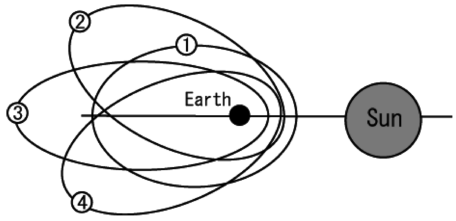

Fig. 3 Librational orbit (hatched region in Fig. 2).

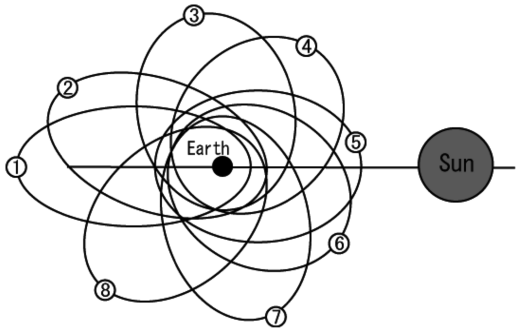

Fig. 4 Rotational orbit (unpatterned region in Fig. 2).

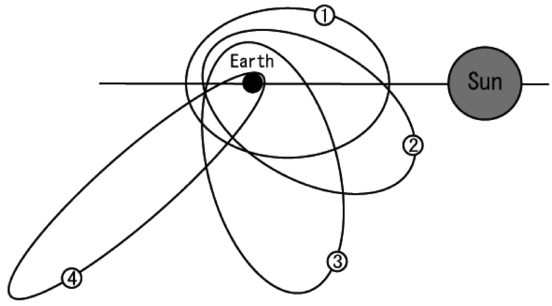

Fig. 5 Unstable orbit (dotted region in Fig. 2).

this example with $\alpha = 0.575$, the characteristic acceleration (a_0) is 0.135 mm/s^2 assuming a semimajor axis of 20 Earth radii.

Orbits in the phase space can be classified into three types: librational, rotational, and unstable orbits, as shown in Fig. 2. The motion in terms of eccentricity ($\bar{k}$) and sun line ($\bar{\gamma}$) coordinates is indicated by arrows in $\bar{k} - \bar{\gamma}$ phase space.

The librational motion is observed in the hatched region of the $\bar{k} - \bar{\gamma}$ phase-space diagram in Fig. 2. The orbits depict a closed loop (numbered 1–4) in the hatched region, and both $\bar{k}$ and $\bar{\gamma}$ are periodic functions of time with the same frequency. Therefore, the perigee of the solar-sail orbit tracks the sun direction, resulting in a reciprocally stretched and contracted orbital shape in terms of both eccentricity and the argument of perigee (Fig. 3). The numbers in Fig. 3 correspond to those in the librational region (hatched) in Fig. 2. The equilibrium point in this libration region can be found by setting the right-hand side of Eqs. (8) and (9) to zero yielding the equilibrium point ($\bar{k}_0, \bar{\gamma}_0$):

$$\bar{k}_0 = \frac{1}{\sqrt{1+\alpha^2}} \qquad \bar{\gamma}_0 = 0$$

At the equilibrium point, the secular change of eccentricity becomes zero and the apse line of the orbit is strictly synchronized to the Earth–sun line, which corresponds to the proposed Geosail orbit [9].

The rotational motion corresponds to the unpatterned region in Fig. 2, where $\bar{\gamma}$ continues to decrease. The perigee of the orbit is left behind by the sun direction along with the deformation of the orbital shape as in Fig. 4.

The separatrix between the librational and the rotational regions contains the zero eccentricity point $(1, \pi)$. H' for the separatrix can be obtained by substituting $\bar{k} = 1$ and $\bar{\gamma} = \pi$ into Eq. (12), which gives $H' = -1$. The separatrix is then obtained by substituting -1 into H' of Eq. (12) to give

$$\cos\bar{\gamma} = \frac{1}{\alpha}\sqrt{\frac{1-\bar{k}}{1+\bar{k}}}$$

The unstable regions are included in the dotted areas in Fig. 2. The unstable orbits reach $\bar{k} = 0$, that is, $\bar{e} = 1$. Hence, orbits in the unstable region reach the parabolic state. An example of the unstable case is plotted in Fig. 5.

The separatrix between the rotational and unstable regions contains the point (0,0). H' for this separatrix is $-\alpha$, which is given by substituting the point (0,0) into $(\bar{k}, \bar{\gamma})$ of Eq. (12), resulting in the following expression for this separatrix:

$$\cos\bar{\gamma} = \frac{\alpha - \bar{k}}{\alpha\sqrt{1-\bar{k}^2}} \tag{13}$$

The two separatrices approach each other as α becomes larger and overlap at $\alpha = 1$. This corresponds to a characteristic acceleration of 0.235 mm/s^2, assuming a semimajor axis of 20 Earth radii. Figure 6 shows the phase-space diagram for $\alpha = 1$. The rotational region disappears in this case, and the separatrix between the librational and unstable orbit is given by

$$\cos\bar{\gamma} = \sqrt{\frac{1-\bar{k}}{1+\bar{k}}} \tag{14}$$

The two separatrices finally overlap when α exceeds 1. Figure 7 shows the phase-space diagram for $\alpha = 1.5$, indicating that stable rotation orbits disappear and are replaced by unstable librational orbits at the unpatterned region. This condition corresponds to a characteristic acceleration of 0.352 mm/s^2, assuming a semimajor axis of 20 Earth radii. In this case, Eq. (13) represents the separatrix between the stable librational and unstable librational regions, and Eq. (14) represents the separatrix between the unstable librational and unstable regions.

The limiting case of $\alpha = \infty$ is shown in Fig. 8. The limiting case corresponds to an infinite characteristic acceleration and yields no stable orbits. All of the solar-sail orbits arrive at $\bar{k} = 0$; that is, $\bar{e} = 1$.

IV. Time Equation

So far, we have focused on the evolution of the orbital shape. In this section, the time equation for the eccentricity parameter $\bar{k}$ and the period of closed orbits (i.e., librational orbits) in the phase space are derived as follows. The period in this case is not that of one revolution around the primary body (i.e., the Earth), but of one

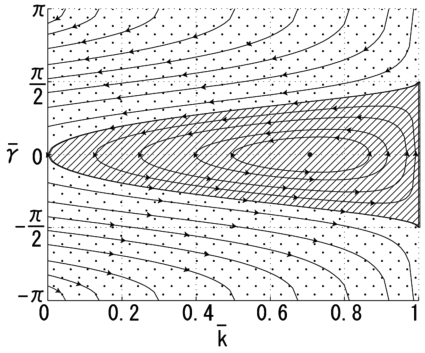

Fig. 6 Eccentricity argument of perigee phase-space diagram ($\alpha = 1$), showing librational (hatched), and unstable (dotted) orbital regions.

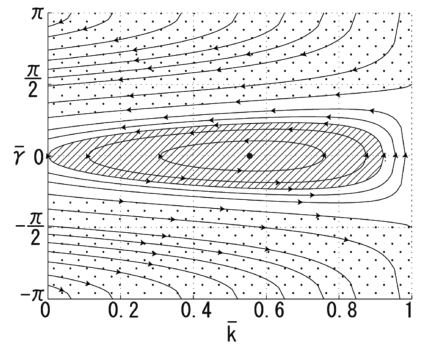

Fig. 7 Eccentricity argument of perigee phase-space diagram ($\alpha = 1.5$), showing stable librational (hatched), unstable librational (unpatterned), and unstable (dotted) orbital regions.

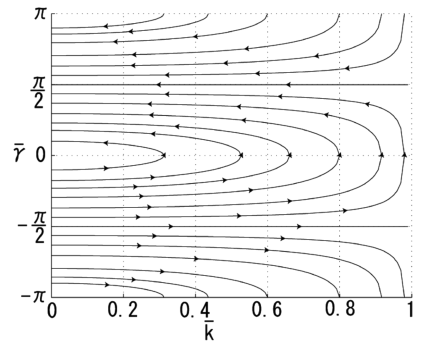

Fig. 8 Eccentricity argument of perigee phase-space diagram ($\alpha = \infty$), showing unstable orbital regions.

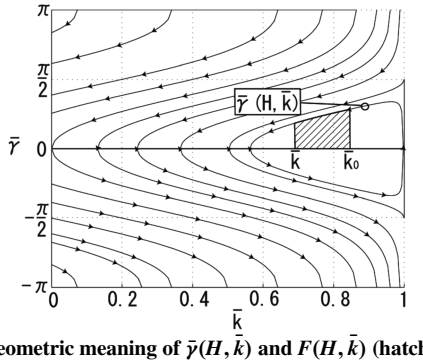

Fig. 9 Geometric meaning of $\bar{\gamma}(H, \bar{k})$ and $F(H, \bar{k})$ (hatched area).

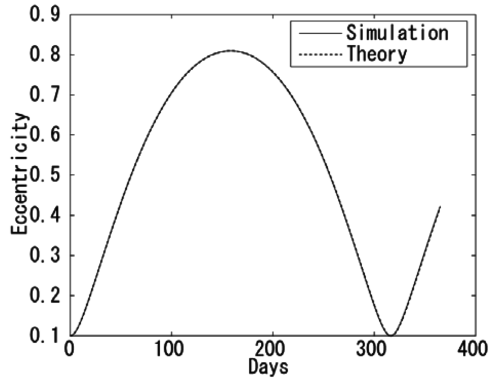

Fig. 10 Theoretical and numerical results for the eccentricity evolution (librational orbit).

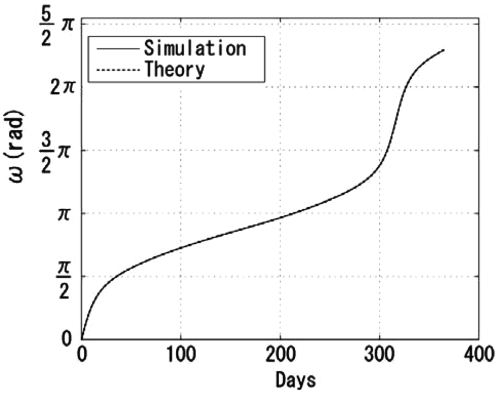

Fig. 11 Theoretical and numerical results for the argument of the perigee evolution (librational orbit).

revolution in the $\bar{k} - \bar{\gamma}$ phase space, which may be considered the sum of orbital periods starting from some point in the phase space to that with the same eccentricity and sun line angle (e.g., sum of orbital periods of orbits 1–4 in Fig. 2 in the hatched region).

First, consider $F(H, \bar{k})$:

$$F(H, \bar{k}) = \int_{k_0}^{k} \bar{\gamma}(H, \bar{k})\, \mathrm{d}\bar{k} = \int_{k_0}^{k} \bar{\gamma}[H, \bar{k}(t)] \frac{\mathrm{d}\bar{k}}{\mathrm{d}t}\, \mathrm{d}t \tag{15}$$

Here $\bar{\gamma}$ denotes the curves in Figs. 2 and 9, and $F(H, \bar{k})$ represents the area of closed orbits as shown in Fig. 9. Substitution of Eq. (9) in Eq. (15) and differentiation with respect to H yields the following time equation:

$$\frac{\partial F}{\partial H} = -\int_{k_0}^{k} \frac{\partial \bar{\gamma}}{\partial H} \frac{\partial H}{\partial \bar{\gamma}}\, \mathrm{d}t = -\int_{t_0}^{t} \mathrm{d}t = -(t - t_0) \tag{16}$$

The time equation for $\bar{k}$ can then be derived from Eqs. (15) and (16) as follows:

$$\begin{aligned} t - t_0 &= -\frac{\partial}{\partial H} \int_{k_0}^{k} \bar{\gamma}(H, \bar{k})\, \mathrm{d}\bar{k} \\ &= \frac{1}{\beta_0 \sqrt{1 + \alpha^2}} \left\{ \arccos \frac{(1 + \alpha^2)\bar{k} + H'}{\alpha \sqrt{1 + \alpha^2 - H'^2}} \right. \\ &\quad \left. - \arccos \frac{(1 + \alpha^2)\bar{k}_0 + H'}{\alpha \sqrt{1 + \alpha^2 - H'^2}} \right\} \end{aligned} \tag{17}$$

Equation (17) gives $\bar{k}$, that is, the eccentricity of the orbit at an arbitrary instant.

The periods of the librational orbits are twice the time between the two intersections of the curve $\bar{\gamma}(H, \bar{k})$ with $\bar{\gamma} = 0$ in the phase space. The values of $\bar{k}$ at the two intersections, $\bar{k}_{\pm}$, are obtained by setting γ to zero in Eq. (12), giving the relation

$$\bar{k}_{\pm} = \frac{-H'}{1 + \alpha^2} \pm \frac{\alpha}{1 + \alpha^2} \sqrt{1 + \alpha^2 - H'^2}$$

Substituting k_+ and k_- for k_0 and k in Eq. (17) gives the following result for the period of closed orbits:

$$T = \frac{2\pi}{\beta_0\sqrt{1+\alpha^2}} \tag{18}$$

Equation (18) indicates that all of the closed orbits in phase space have the same period. Hence, the periods of the closed orbits in the $\bar{k} - \bar{\gamma}$ phase space are dependent only on the solar pressure parameter (α) as a function of the characteristic acceleration (a_0) and semimajor axis ($\bar{a}$). Assuming $\alpha = 0.575$, the period in the phase space is 317 days.

V. Comparison with Numerical Simulations

The analysis derived here is based on a time averaging approach. In justification of this approximation, the averaged evolution of the solar-sail orbit can be compared with that obtained by a fourth-order Runge–Kutta numerical integration using the equations of motion in Cartesian coordinates taking the solar radiation force and a single gravitational field, the Earth, into account. The initial parameter values for the librational orbits, adopted as a representative case, are summarized as follows: $\alpha = 0.575$, $\bar{a} = 1.0$, $e = 0.1$, and $\omega = 0.0$. Figures 10 and 11 compare the results of the two approaches in terms of the temporal evolution of eccentricity and the argument of perigee. The period of the librational motion is 317 days (see Fig. 10), which coincides with that calculated by Eq. (18). The coincidence of the two results suggests that the present approximation is valid. The orbital dynamics considering lunisolar gravitational perturbations and higher-order geopotential are justified next.

VI. Mission Application

The present analysis of the long-term dynamics of the solar-sail orbit using averaged Lagrange's equations can be applied to the geomagnetic tail exploration mission under solar-sail propulsion.

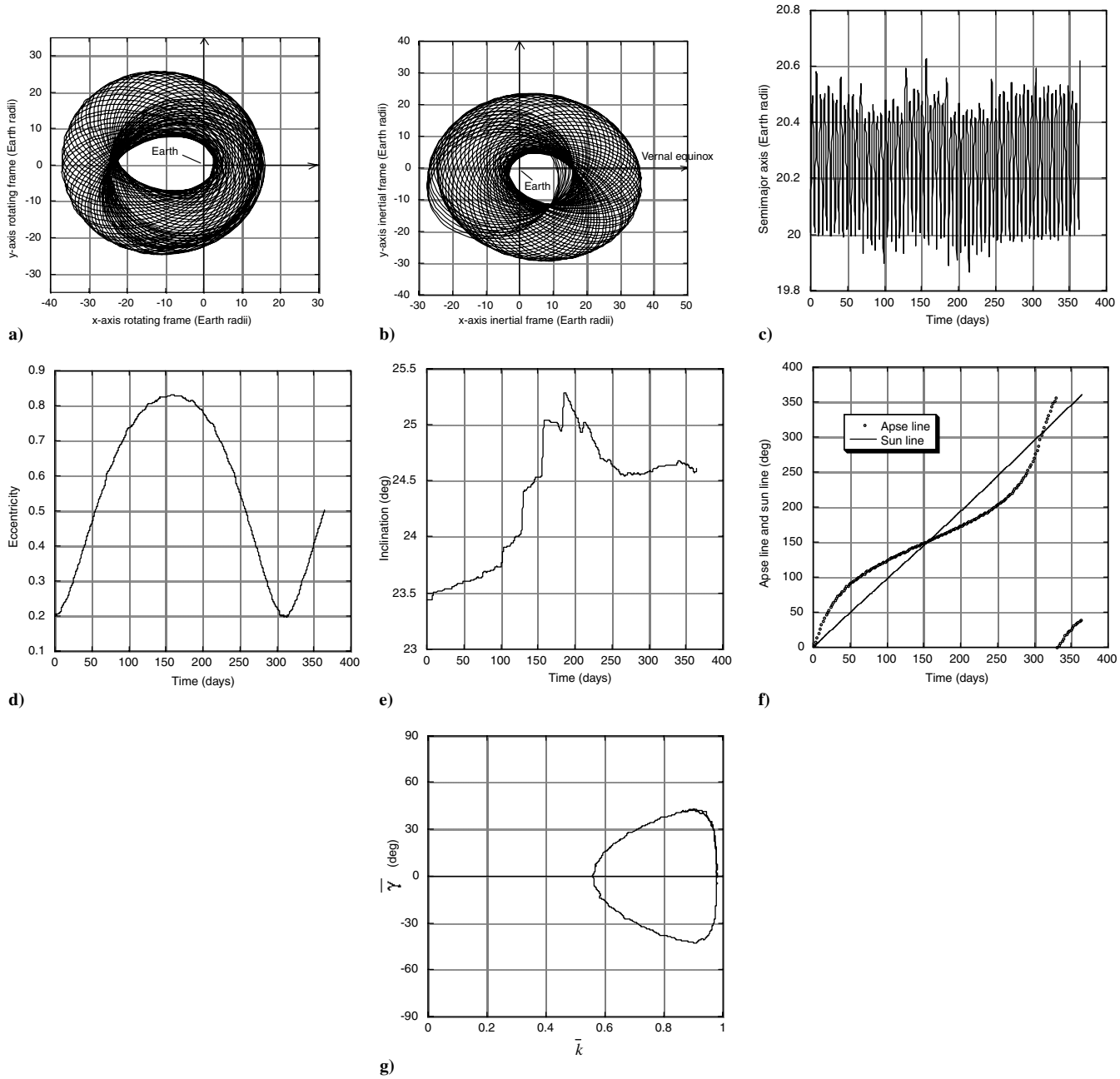

Fig. 12 a) Evolution of librational Geosail orbit in rotating frames fixed to the sun–Earth line. b) Evolution of librational Geosail orbit in Earth-centered inertial coordinates. c) Semimajor axis of librational Geosail orbit. d) Eccentricity of librational Geosail orbit. e) Inclination of librational Geosail orbit. f) Apse line (ω) and sun line (Σ) over 1 year for librational Geosail orbit. g) $\bar{k} - \bar{\gamma}$ phase–space trajectory of librational Geosail orbit.

The Geosail mission [9] uses the equilibrium eccentricity orbit in the $\bar{k}-\bar{\gamma}$ phase space. Using the present analysis extended to the global behavior of the Earth-orbiting solar-sail orbits, it may be possible to increase the scientific return of the Geosail mission. In the librational region of $\bar{k}-\bar{\gamma}$ phase space, the eccentricity of the satellite orbits changes while the perigee chases the sun direction.

A Geosail orbit with variable eccentricity could be designed as follows. Given two extreme eccentricities, e_1 and e_2, the characteristic acceleration a_0 can be expressed as follows according to Eq. (10):

$$a_0 = \frac{2}{3}\frac{\beta_0}{\sqrt{\bar{a}}(e_2-e_1)}\left(\sqrt{1-e_1^2}-\sqrt{1-e_2^2}\right) \tag{19}$$

Here recall that H is constant, and the perigee direction is assumed to be directed sunward (i.e., $\gamma = 0$). Taking the limit as e_1 tends to e_2 in Eq. (19), Eq. (19) reduces to

$$a_0 = \frac{2}{3}\beta_0\frac{e_2}{\sqrt{1-e_2^2}}\frac{1}{\sqrt{\bar{a}}} \tag{20}$$

This result is identical to Eq. (9) of MacInnes et al. [9]. Assuming a 10×30 Earth radii mission ($\bar{a}=20$ Earth radii) with constant eccentricity of $e_2 = 0.5$, the required characteristic acceleration determined by Eq. (20) is 0.135 mm/s^2. This required characteristic acceleration becomes smaller as the semimajor axis increases.

A librational orbit for a solar-sail mission involving geomagnetic tail exploration may be numerically exemplified as follows. Assuming a semimajor axis $\bar{a}$ of 20 Earth radii and two extreme eccentricities of 0.2 and 0.8, Eq. (19) yields a characteristic acceleration a_0 of 0.148 mm/s^2, and Eq. (11) indicates a solar pressure parameter a of 0.631. As $\alpha < 1$, the $\bar{k}-\bar{\gamma}$ phase-space diagram resembles that in Fig. 2, with librational, rotational, and unstable orbits available depending on the initial conditions in phase space. A simulation of a librational orbit with a sun-pointing steering law is shown in Fig. 12. This simulation starts from a 16×24 Earth radii orbit with eccentricity of 0.2 over a 1-year duration. The initial perigee direction is aligned with the sun direction (i.e., $\gamma = 0$). Lunar and solar gravitational perturbations and an order 5×5 geopotential model are included. An integrator with multistep predictor–corrector method is used in Earth-centered inertial coordinates. The sail is assumed to have a total reflectivity of 80%, an area of 1444 m^2, and a total mass of 80 kg, providing the required sail characteristic acceleration of 0.148 mm/s^2 at a solar pressure of 4.56×10^{-6} Nm^{-2} at a distance of 1 AU. The mission is assumed to start at the spring equinox (21 March 2010) with an equatorial inclination of 23.4 deg, corresponding to an orbit within the ecliptic plane. Figure 12 shows that the perigee direction chases the sun line in librational motion, and the eccentricity varies from 0.2 to ca. 0.8 as designed in the presence of these perturbations. These dynamics can also be observed in the eccentricity argument of perigee ($\bar{k}-\bar{\gamma}$) phase space. There exists a small perturbation of the semimajor axis, and a slow secular perturbation of the orbit inclination due to lunar and solar perturbations. These results demonstrate that the phase-space approach remains valid in the presence of lunisolar gravitational perturbations as well as a higher-order geopotential. Flexibility of mission design can thus be achieved by allowing eccentricity variation.

VII. Conclusions

The long-term dynamics of an Earth-orbiting solar sail was derived by averaging the Lagrange's planetary equations constituting a Hamiltonian system, assuming that the sail normal is directed sunward. The solar-sail orbits were classified into three types in the eccentricity argument of perigee phase space. For a small solar pressure parameter (i.e., small characteristic acceleration), librational, rotational, and unstable orbits are apparent in the phase space. The argument of the perigee of librational orbits tracks the sun direction, whereas that for rotational orbits fails to maintain and is left behind the sun direction. Unstable orbits eventually result in parabolic orbits. The dynamics in the eccentricity argument of perigee phase space is dependent on the solar pressure parameter, which represents the acceleration due to solar radiation pressure. A time equation and the period of orbit deformation were also obtained. The averaging theory was confirmed to be valid by comparison with numerically integrated orbits. Derivation of averaged equations was also shown to be possible by canonical perturbation theory substantially reducing the manipulations required for averaging. Finally, the librational orbits in the eccentricity argument of perigee phase space were applied to the design of the geomagnetic tail observation under solar sailing propulsion.

Appendix: Canonical Transformation Approach

The averaged Hamiltonian for solar-sail dynamics is alternatively derived by a canonical transformation approach.

I. Action-Angle Variables

For canonical transformation, canonical variables satisfying the canonical equations of the Hamilton are employed [13] as follows:

$$\dot{\boldsymbol{q}} = \frac{\partial H(\boldsymbol{q},\boldsymbol{p})}{\partial \boldsymbol{p}} \qquad \dot{\boldsymbol{p}} = -\frac{\partial H(\boldsymbol{q},\boldsymbol{p})}{\partial \boldsymbol{q}}$$

Here $\boldsymbol{q} = (q_1, q_2, \ldots, q_n)$ and $\boldsymbol{p} = (p_1, p_2, \ldots, p_n)$ are the generalized coordinates and momenta of the system, respectively, and $H(\boldsymbol{q},\boldsymbol{p})$ represents the Hamiltonian of the system.

The transformation from the old coordinate set $(\mathbf{q},\mathbf{p})$ to the new coordinate set $(\mathbf{Q},\mathbf{P})$ is canonical when the new coordinate set satisfies the canonical equations of the Hamilton with a new Hamiltonian K [14]. The action-angle variable set is a useful canonical variable set for treating periodic motion. The action variables J_i are defined by

$$J_i = \oint p_i(H_i, q_i)\,\mathrm{d}q_i$$

where the system is considered completely separable, that is,

$$H(\boldsymbol{q},\boldsymbol{p}) = \sum_i H_i(q_i, p_i)$$

and the integration is performed along one orbit of a periodic system in the $q_i - p_i$ phase plane. The angle variables w_i, which are conjugate to the action variables, are defined by

$$\dot{w}_i = \frac{\partial H_i}{\partial J_i}$$

The action variables and a subset of the angle variables are constants of the system, with the remaining angle variables varying linearly with time. The transformation to action variables is constructed such that the new Hamiltonian K is zero.

The classical Keplarian orbital elements such as the semimajor axis and the eccentricity are not canonical variables. Although these variables represent the shape of orbits directly, canonical sets of variables called Delaunay variables [15] are introduced, which are equivalent to action-angle variables. The relation between the Keplerian orbital elements (a, e, ω, M) and the Delaunay variables (J_1, J_2, ω, M) are defined by

$$J_1 = \sqrt{a(1-e^2)} \tag{A1}$$

$$J_2 = \sqrt{a} \tag{A2}$$

where the canonical sets are (J_1, ω) and (J_2, M), and M is the mean anomaly. Although these variables are not intuitive, the use of these variables is advantageous for canonical transformation.

II. Canonical Perturbation Theory

Canonical perturbation theory [16] can be applied when a small perturbation is added to a well-known system. Let $H_0(\boldsymbol{q}, \boldsymbol{p}, t)$ represent the Hamiltonian for the solvable, unperturbed Hamilton system, which is defined in terms of sets of action-angle variables $(\boldsymbol{J}, \boldsymbol{w})$, where $\boldsymbol{J}$ and $\boldsymbol{w}$ are the vector forms of the action variables and angle variables, respectively. When the transformation from $(\boldsymbol{p}, \boldsymbol{q})$ to $(\boldsymbol{J}, \boldsymbol{w})$ is applied to $H_0(\boldsymbol{q}, \boldsymbol{p}, t)$, the new Hamiltonian $K_0(\boldsymbol{J}, \boldsymbol{w}, t)$ becomes zero. Therefore, if a small perturbation Hamiltonian $\Delta H(\boldsymbol{q}, \boldsymbol{p}, t)$ is added to the unperturbed system and the transformation to $(\boldsymbol{J}, \boldsymbol{w})$ is applied, the transformed Hamiltonian is obtained as

$$K(\boldsymbol{J}, \boldsymbol{w}, t) = \Delta H(\boldsymbol{J}, \boldsymbol{w}, t)$$

The new canonical equations are then given by

$$\dot{\boldsymbol{J}} = -\frac{\partial \Delta H(\boldsymbol{J}, \boldsymbol{w}, t)}{\partial \boldsymbol{w}} \qquad \dot{\boldsymbol{w}} = \frac{\partial \Delta H(\boldsymbol{J}, \boldsymbol{w}, t)}{\partial \boldsymbol{J}}$$

The Delaunay variables J_1, J_2, and ω are invariant, and M increases linearly with time without perturbations. M is thus proportional to time as follows:

$$M = \frac{t}{J_2^3}$$

When a perturbation is so small that the change in these variables in one period is negligible, the averaged Hamiltonian $\overline{\Delta H}(\bar{J}_1, \bar{J}_2, \bar{\omega})$ can be computed as follows:

$$\overline{\Delta H}(\bar{J}_1, \bar{J}_2, \bar{\omega}) = \frac{1}{\tau}\int_0^{\tau} \Delta H[\bar{J}_1, \bar{J}_2, \bar{\omega}, \bar{M}(t), t]\,\mathrm{d}t \tag{A3}$$

Here, τ represents the period of the system under consideration, and the overbars on the Delaunay variables represent averages. The averaged Hamiltonian generates the following averaged canonical equations:

$$\dot{\bar{J}}_1 = -\frac{\partial \overline{\Delta H}}{\partial \bar{\omega}} \qquad \dot{\bar{J}}_2 = -\frac{\partial \overline{\Delta H}}{\partial \bar{M}} \qquad \dot{\bar{\omega}} = \frac{\partial \overline{\Delta H}}{\partial \bar{J}_1}$$

III. Averaged Hamiltonian of Solar Radiation Pressure

The solar radiation pressure in Cartesian coordinates is given by

$$f_x = -a_0 \cos \beta_0 t \tag{A4}$$

$$f_y = -a_0 \sin \beta_0 t \tag{A5}$$

where f_x and f_y represent the x and y components of solar radiation pressure. The perturbative Hamiltonian corresponding to the solar radiation pressure given by Eqs. (A4) and (A5) then becomes

$$\Delta H(x, y) = a_0 x \cos \beta_0 t + a_0 y \sin \beta_0 t \tag{A6}$$

Equation (A6) can be confirmed to give the force due to solar radiation pressure by differentiating with respect to x and y. Transformation of Eq. (A6) to polar coordinates leads to the following expression for the Hamiltonian:

$$\Delta H(r, \theta) = a_0 r \cos\theta \cos \beta_0 t + a_0 r \sin\theta \sin \beta_0 t$$

The relation between the distance r and the Delaunay variables is expressed by [17]

$$r = \frac{J_1^2}{1 + \sqrt{1 - (\frac{J_1}{J_2})^2}\cos(\theta - \omega)} \tag{A7}$$

where θ is related to M by [17]

$$M = \psi - e \sin \psi \tag{A8}$$

$$\tan\frac{\theta}{2} = \sqrt{\frac{1+e}{1-e}}\tan\frac{\psi}{2} \tag{A9}$$

Here, ψ is an intermediate variable (eccentric anomaly) connecting θ and M. The Hamiltonian can then be expressed in terms of the Delaunay variables using Eqs. (A7–A9):

$$\Delta H(J_1, J_2, \omega, M, t) = a_0 r[J_1, J_2, \theta'(M)]\cos[\theta'(M) + \omega - \beta_0 t] \tag{A10}$$

where $\theta'(M) = \theta - \omega$. Equation (A10) is a time-dependent Hamiltonian. The canonical transformation $\bar{\gamma} = \bar{\omega} - \beta_0 t$ of Eq. (A10) yields a manageable autonomous Hamiltonian system. Consider the canonical equation of $\bar{\gamma}$ with the aid of the canonical equation of ω:

$$\dot{\bar{\gamma}} = \dot{\bar{\omega}} - \beta_0 = \frac{\partial(\Delta H - \beta_0 J_1)}{\partial J_1}$$

$\Delta H - \beta_0 J_1$ can thus be regarded as a new Hamiltonian $\Delta H'(J_1, J_2, \gamma, M)$:

$$\Delta H'(J_1, J_2, \gamma, M) = a_0 r[J_1, J_2, \theta'(M)]\cos[\theta'(M) + \gamma] - \beta_0 J_1$$

After this transformation, the new canonical variables sets are (J_1, γ) and (J_2, M).

Last, the Hamiltonian averaging given by Eq. (A3) is applied to $\Delta H'$. The integration is performed with respect to true anomaly instead of time using the conservation of angular momentum, resulting in the following averaged Hamiltonian:

$$\begin{aligned}\overline{\Delta H}(\bar{J}_1, \bar{J}_2, \bar{\omega}, t) &= \frac{1}{2\pi \bar{J}_2^3}\int_0^{2\pi}\{a_0 r \cos[\theta'(\bar{M}) + \bar{\gamma}] - \beta_0 \bar{J}_1\}\frac{r^2}{\bar{J}_1}\mathrm{d}\theta' \\ &= \overline{J_2}\left[-\frac{3}{2}a_0 \bar{J}_2 \sqrt{1 - \left(\frac{\bar{J}_1}{\bar{J}_2}\right)^2}\cos\bar{\gamma} - \beta_0 \frac{\bar{J}_1}{\bar{J}_2}\right]\end{aligned}$$

As the averaged Hamiltonian does not contain $\bar{M}$, the conjugate momentum $\bar{J}_2$ is constant, that is, the semimajor axis is given by $\sqrt{a}$. This Hamiltonian derived from the canonical transformation is equivalent to that derived from the direct averaging of the Lagrange's equation (10). This equivalence can be demonstrated using the relation

$$\bar{k} = \frac{\bar{J}_1}{\bar{J}_2}$$

which can be derived from Eqs. (A1) and (A2).

References

[1] McInnes, C. R., *Solar Sailing: Technology, Dynamics and Mission Applications*, Springer–Verlag, London, 1999, pp. 19–31.

[2] Colasurdo, G., and Casalino, L., "Optimal Control Law for Interplanetary Trajectories with Nonideal Solar Sail," *Journal of Spacecraft and Rockets*, Vol. 40, No. 2, 2003, pp. 260–265.

[3] Circi, C., "Mars and Mercury Missions Using Solar Sails and Solar Electric Propulsion," *Journal of Guidance, Control, and Dynamics*, Vol. 27, No. 3, 2004, pp. 496–498.

[4] Mengali, G., and Quarta, A., "Optimal Three-Dimensional Interplanetary Rendezvous Using Non-Ideal Solar Sail," *Journal of Guidance, Control, and Dynamics*, Vol. 28, No. 1, 2005, pp. 173–177.

[5] Hughes, G., and McInnes, C. R., "Small-Body Encounters Using Solar Sail Propulsion," *Journal of Spacecraft and Rockets*, Vol. 41, No. 1, 2004, pp. 140–150.

[6] Bookless, J., and McInnes, C. R., "Dynamics and Control of Displaced Periodic Orbits Using Solar-Sail Propulsion," *Journal of Guidance, Control, and Dynamics*, Vol. 29, No. 3, 2006, pp. 527–537.

[7] McInnes, C. R., and Simmons, J. F. L., "Solar Sail Halo Orbits Part 2—Geocentric Case," *Journal of Spacecraft and Rockets*, Vol. 29, No. 4, 1992, pp. 472–479.

[8] Baoyin, H., and McInnes, C. R., "Solar Sail Orbits at Artificial Sun-Earth Libration Points," *Journal of Guidance, Control, and Dynamics*,

Vol. 28, No. 6, 2005, pp. 1328–1331.
[9] McInnes, C. R., Macdonald, M., Angelopolous, V., and Alexander, D., "GEOSAIL: Exploring the Geomagnetic Tail Using a Small Solar Sail," *Journal of Spacecraft and Rockets*, Vol. 38, No. 4, 2001, pp., 622–629.
[10] MacDonald, M., and McInnes, C. R., "Geosail: An Enhanced Magnetospheric Mission Using a Small Low Cost Solar Sail," IAF Paper 00-W.1.06., Oct. 2000.
[11] Uesugi, K., Kawaguchi, J., Ishii, N., Yamakawa, H., Terada, H., and Matsuoka, M., "GEOTAIL Launch Window Expansion and Trajectory Correction Strategies: Analysis and Flight Results," *5th International Space Conference of Pacific-Basin Societies*, Chinese Society of Astronautics, Shanghai, 6–9 June 1993, pp. 833–847.
[12] Fortescue, P., Stark, J., and Swinerd, G., *Spacecraft Systems Engineering*, 3rd ed., Wiley, New York, 2003, p. 94.
[13] Goldstein, H., Poole, C., and Safko, J., *Classical Mechanics*, Addison Wesley, San Francisco, 2002, Chap. 8, pp. 337, 338.
[14] Goldstein, H., Poole, C., and Safko, J., *Classical Mechanics*, Addison Wesley, San Francisco, 2002, Chap. 9, pp. 369, 370.
[15] Goldstein, H., Poole, C., and Safko, J., *Classical Mechanics*, Addison Wesley, San Francisco, 2002, Chap. 10, pp. 466–477.
[16] Goldstein, H., Poole, C., and Safko, J., *Classical Mechanics*, Addison Wesley, San Francisco, 2002, Chap. 12, pp. 527–533.
[17] Goldstein, H., Poole, C., and Safko, J., *Classical Mechanics*, Addison Wesley, San Francisco, 2002, Chap. 3, pp. 95–102.

B. Marchand
Associate Editor